RESEARCH ARTICLE

A framework for risk assessment of groundwater contamination integrating hydrochemical, hydrogeological, and electrical resistivity tomography method

Jian Meng[1] · Kaiyou Hu[2] · Shaowei Wang[1] · Yaxun Wang[1] · Zifang Chen[3] · Cuiling Gao[4] · Deqiang Mao[1]

Abstract

Groundwater contamination have been widely concerned. To reliably conduct risk assessment, it is essential to accurately delineate the contaminant distribution and hydrogeological condition. Electrical resistivity tomography (ERT) has become a powerful tool because of its high sensitivity to hydrochemical parameters, as well as its advantages of non-invasiveness, spatial continuity, and cost-effectiveness. However, it is still difficult to integrate hydrochemical, hydrogeological, and ERT datasets for risk assessment. In this study, we develop a general framework for risk assessment by sequentially jointing hydrochemical, hydrogeological, and ERT surveys, while establishing petrophysical relationships among these data. This framework can be used in groundwater-contaminated site and help to delineate the distribution of contaminants. In this study, it was applied to a nitrogen-contaminated site where field ERT survey and borehole information provided valuable measurement data for validating the consistency of contamination and hydrogeological condition. Risk assessment was conducted based on the refined results by the establishment of relationship between conductivity and contaminants concentration with $R^2 > 0.84$. The contamination source was identified and the transport direction was predicted with the good agreement of $R^2 = 0.965$ between simulated and observed groundwater head, which can help to propose measures for anti-seepage and monitoring. This study thus enhances the reliability of risk assessment and prediction through a thought-provoking innovation in the realm of groundwater environmental assessment.

Keywords Groundwater · Risk assessment · Geophysics method · Pollution · Spatial distribution · Prediction

Introduction

Groundwater is a vital freshwater resource for maintaining domestic life, industrial and agricultural production, and ecological function. Globally, over 1.5 billion people rely on groundwater as their primary source for drinking, irrigation,

✉ Deqiang Mao
  maodeqiang@sdu.edu.cn

  Jian Meng
  mengjiansdu@163.com

  Kaiyou Hu
  HKY201426@163.com

  Shaowei Wang
  shaoweiwang@sdu.edu.cn

  Yaxun Wang
  yaxun_w@163.com

  Zifang Chen
  chenzf0716@126.com

  Cuiling Gao
  124486040@qq.com

1 School of Civil Engineering, Shandong University, Jinan 250061, China

2 Kunming Engineering Corporation Limited, Kunming 650051, China

3 Shandong Institute of Eco-Environmental Planning, Jinan 250101, China

4 Shandong Institute for Production Quality Inspection, Jinan 250102, China

and industrial purposes (Sankoh et al. 2023). However, it is potentially vulnerable to the contaminants like inorganic salts, heavy metals, and organic compounds during human activity (Siddiqua et al. 2022). In 202 cities across China, groundwater from 61.5% of the 4896 monitoring wells could not be directly utilized (Han et al. 2016). The risk of groundwater contamination was more likely to affect industrial and agricultural production and even human health (Hou et al. 2023). For example, the overuse of fertilizers in agriculture or leaks from inorganic fertilizer plant may cause nonpoint and point groundwater contamination of total nitrogen (TN) and total phosphorus (TP) (Lawniczak et al. 2016). These contaminants in groundwater environment have been proved to decrease soil fertility, reduce crop yields, and even increase human cancer risk (Rogers et al. 2023). In addition, petrochemicals derived from petroleum are well known for their toxicity and carcinogenic risks to humans (Yu et al. 2015). The hexavalent chromium present in industrial wastes also lead to health effects such as pulmonary congestion, vomiting, and liver damage (Karunanidhi et al 2021).

Faced with such a serious situation of groundwater contamination, a series of legislation and standardization have been enacted to enhance groundwater protection (Li et al. 2017). However, risk assessment of the groundwater environment remains a challenge because of the invisibility and uncertainty of groundwater contamination. The heterogeneity of porous medium distribution makes it difficult to map the groundwater flow and contaminant transport (de Barros et al. 2016). Therefore, the accurate hydrogeology, hydrochemical, and contamination information is beneficial to risk assessment and numerical simulation of solute transport (Fu et al. 2019).

The acquirement of site information requires the use of many boreholes to reduce the uncertainty between them and make it expensive and time consuming (Meng et al. 2022b). Traditional borehole sampling techniques for delineating groundwater contamination are primarily based on intrusive drilling methods to acquire measurements on a small scale (Xia et al. 2021). The drawbacks of these methods may be mitigated using electrical resistivity tomography (ERT), which is a non-intrusive geophysical method based on electrical property difference of subsurface medium (Binley and Slater 2020).

ERT is a frequently utilized and well-established method for geophysical exploration (Balasco et al. 2022). It is widely used in the field of environmental investigation (Mary et al. 2023), hydrogeological survey (Mao et al. 2022), groundwater vulnerability assessment (Akiang et al. 2023), and seawater intrusion (Kumar et al. 2023). It has been applied to map structures from the decimeter scale to kilometers (Binley and Slater 2020). However, one of the main weaknesses of this method is the survey resolution decreases rapidly with depth (Loke et al. 2010). The depth of investigation (DOI) is

limited to a specific depth based on measurement data size. The improvement of DOI is accompanied by an increase in the size of raw data, thus increasing the survey time. To balance DOI and survey time, the arrays selected for ERT survey need to be determined based the interesting depth of groundwater contamination at each site. ERT is an indirect method because resistivity is determined by many factors such as water content, porosity, and grain size (Binley and Slater 2020). Therefore, it is essential to verify the ERT results using borehole or monitoring well data (Meng et al. 2022a). Given these challenges, current research persists in relying predominantly on discontinuous and intrusive borehole to furnish information for risk assessment (Akiang et al. 2023). It is therefore desirable to develop new frameworks that can effectively conduct risk assessment for leveraging the advantages of ERT.

The purpose of this study is to develop such a framework for risk assessment of groundwater contamination integrating hydrochemical, hydrogeological, and ERT method. The ERT result can be interpreted in conjunction with hydrochemical and hydrogeological data by establishing petrophysical relationships among resistivity and contamination concentration or other parameters within this framework. This integration enhances the reliability of risk assessment and prediction. The proposed framework includes borehole investigation, ERT survey, hydrogeology structure and contamination distribution delineation, and contaminant transport modeling and predicting. We introduced the theoretical background of framework and how to apply it. Finally, a risk assessment of nitrogen-contaminated site was carried out to demonstrate the use of our proposed framework.
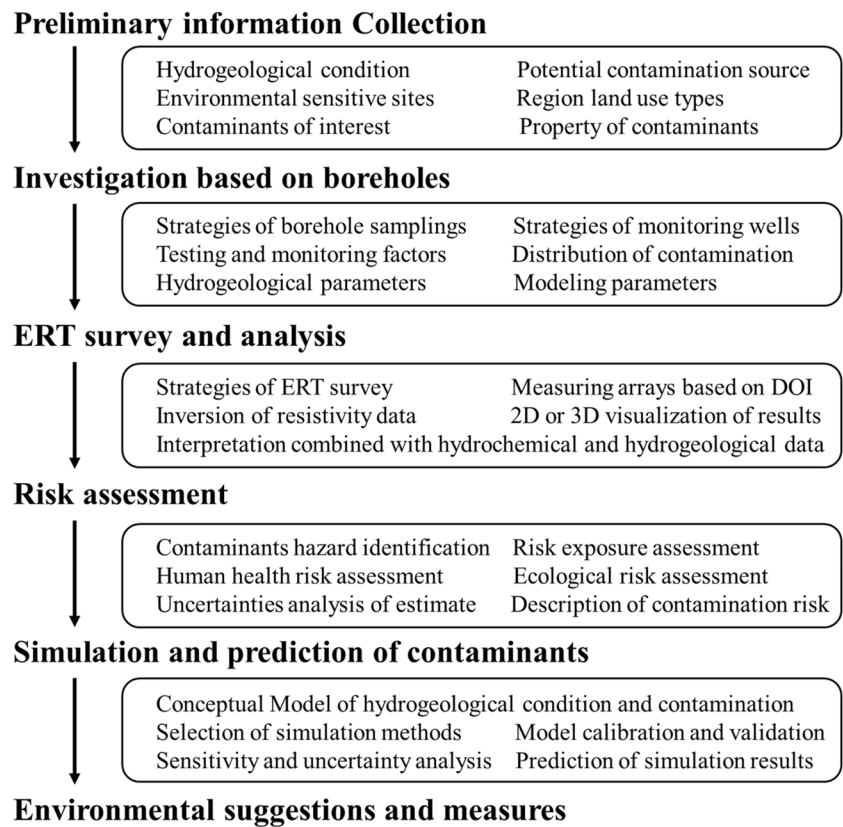
A general framework for risk assessment

In this section, we proposed a general framework for risk assessment of groundwater contamination integrating hydrochemical, hydrogeological analysis, and ERT method (Fig. 1). Both borehole investigation and ERT survey are considered in this framework. To increase the reliability and accuracy of risk assessment, ERT results are interpreted in conjunction with borehole data. The refined distribution of contaminant concentration is applied to conduct risk assessment. Besides, the hydrogeological condition is revised based on the ERT results and is used as an initial condition for simulation and prediction of contaminants. The proposed framework is outlined in Fig. 1, and the details are discussed as follows.

Background information and borehole investigation

The risk of groundwater is from the balance between groundwater vulnerability and the effect of contaminants

Fig. 1 The framework for risk assessment of groundwater contamination integrating boreholes investigaiton and ERT survey

Preliminary information Collection

Hydrogeological condition	Potential contamination source
Environmental sensitive sites	Region land use types
Contaminants of interest	Property of contaminants

Investigation based on boreholes

Strategies of borehole samplings	Strategies of monitoring wells
Testing and monitoring factors	Distribution of contamination
Hydrogeological parameters	Modeling parameters

ERT survey and analysis

Strategies of ERT survey	Measuring arrays based on DOI
Inversion of resistivity data	2D or 3D visualization of results
Interpretation combined with hydrochemical and hydrogeological data	

Risk assessment

Contaminants hazard identification	Risk exposure assessment
Human health risk assessment	Ecological risk assessment
Uncertainties analysis of estimate	Description of contamination risk

Simulation and prediction of contaminants

Conceptual Model of hydrogeological condition and contamination	
Selection of simulation methods	Model calibration and validation
Sensitivity and uncertainty analysis	Prediction of simulation results

Environmental suggestions and measures

because of human activities (Liu et al. 2019). Furthermore, global climate change has the potential to alter groundwater recharge, groundwater elevations, and consequently groundwater vulnerability (Persaud and Levison 2021). Risk assessment of groundwater contamination is determined by the following three factors: (1) the reasonable data used to reflect the vulnerability and contamination of groundwater, (2) hazard identification and transport prediction of contaminants, (3) credible suggestions and measures for environmental protection and prevention (Calò and Parise 2009).

Firstly, preliminary information is necessary to be collected for knowing the overall situation and deploying the next steps, including hydrogeological condition, potential contamination source, and environmental sensitive sites. The hydrogeological condition can be obtained through conducting large-scale hydrogeological survey or retrieving hydrogeological map. History information and interview with related persons are useful for identifying the potential contamination source, generally including land use and special incident. The environmental sensitive sites can be classified base on the intrinsic vulnerability of the vadose zone and the aquifer (Liu et al. 2019). Contaminants of interest can be speculated by the methods similar to those described above for potential contamination source, and the property of contaminants can be evaluated according to *Standard for Groundwater Quality* (GB/T 14848–2017), *Guidelines for drinking-water quality* (WHO), *National Recommended Water Quality Criteria* (US EPA), or *Environmental quality standards applicable to surface water* (2008/105/EC).

Secondly, the investigation based on borehole is implemented to collect hydrochemical and hydrogeological data. Typically, a borehole survey goes through two stages: preliminary investigation and detailed investigation. The purpose of preliminary investigation is to ascertain the general situation of contamination and to develop the strategies for detailed investigation, and which of detailed investigation is to confirm the type and concentration of contaminants and to locating the spatial distribution. The location and depth of borehole is determined according to preliminary information collection, and the same goes for quality analysis. The concentration data from boreholes are used to delineate the contamination distribution by interpolation or simulation, and furthermore, inferring contamination source and plume. Besides, the hydrogeological tests are conducted aiming to acquire detailed hydrogeological information for simulation and prediction.

ERT survey and analysis

In ERT method, the spatial variation of resistivity is the intrinsic property of subsurface medium reflecting its resistance to electrical current. Electrical resistivity data

is generally collected using four-electrode measurement in field (Xu and Noel 1993). Two electrodes are deployed to create an electrical field, and the potential difference is measured between other two electrodes (Fig. S1a). The measured potential difference (ΔV) is applied combinedly with the injection current (I_{in}) and a geometric factor (K), which is relative to the position of four electrodes, to calculate an apparent resistivity (ρ_a) following Ohm's law (Binley and Slater 2020).

$$\rho_a = K\frac{\Delta V}{I_{in}} \tag{1}$$

When there are underground heterogeneities, the apparent resistivity changes with the electrodes position. The apparent resistivity reflects comprehensively subsurface distribution around electrodes and the real resistivity distribution need to be obtained by inversion using the data sets of measured apparent resistivity. The inversion procedure mainly utilizes the finite element method and the finite difference method (Loke and Barker 1996). According to these methods, underground media is divided into triangular or rectangular grids with precise position and size. The model grids are first assigned an initial value and then resistivity of each grid are adjusted and iterated to achieve agreement between the calculated and measured apparent resistivity values from field surveys (Loke et al. 2003).

ERT survey can be implemented in 2D, 3D, and even 4D, covering scales from decimeters to kilometers (Binley and Slater 2020). The resistivity distribution is different in contaminated and non-contaminated medium, and the resistivity values would change due to contamination concentration, which could help delineate contaminant distribution (Sanuade et al. 2022). Different types of contamination induce distinct resistivity responses depending on the electrical property of the contaminants. For example, groundwater contaminated with inorganic substances show a low resistivity response due to the increase in pore water conductivity caused by dissolved inorganic salts (Maurya et al. 2017). Organic-contaminated media exhibit a high resistivity response because of the substitution of conductive pore water by resistive organic compounds (Mao et al. 2016). In addition, there is a decreasing tendency of resistivity with the increase of heavy metal concentrations in soils attributed to variation of ion concentration and surface conductivity (Chu et al. 2017). In landfill, construction and demolition waste generally shows a high resistivity response, while municipal soil waste normally exhibits a low resistivity response (Flores-Orozco et al. 2020). However, ERT may lack sensitive to low concentration contaminants, as resistivity is also influenced by various factors such as water content, porosity, and grain

size. Therefore, it could be used in conjunction with other geophysical methods or borehole techniques.

Interpretation of ERT results is the process of deriving contamination distribution from resistivity profiles. Resistivity anomaly responses are often used to qualitatively determine whether or not groundwater is contaminated and then are verified by borehole sampling. Furthermore, a quantitative relationship between resistivity and contaminant concentration can be established and the concentration distribution be calculated from the resistivity profiles in some cases (Naudet et al. 2004; Xia et al. 2021). Generally, a linear relationship can be established between resistivity and inorganic contaminant concentration based on Archie's law and its derivation (Archie 1942).

$$\rho_0 = \rho_w \bullet \phi^{-m} \tag{2}$$

where ρ_0 is the resistivity of a saturated material, ρ_w is the resistivity of groundwater, ϕ is the interconnected porosity, and m is the cementation exponent. Archie's law shows that there is a linear relationship between resistivity of saturated media and groundwater. And the resistivity of groundwater is linearly proportional to the concentration of ions, i.e., the concentration of inorganic contaminants. Besides, there is also an approximately linear relationship between organic contaminant concentration and resistivity within a certain concentration range (Naudet et al. 2004). Thus, interpretation of resistivity results with combined hydrochemical data could improve the reliability of groundwater contamination distribution.

Optimized survey design for ERT

In ERT survey, the depth of investigation increases as the separation distance between current and potential electrodes increases. However, the electrode spacing cannot be expanded without limitation. We need take the same electrode distance and obtain deeper characterization into account. The arrangement of four electrodes determines the depth and position of investigation. Therefore, it is necessary to optimize arrays before each survey according to the requirement of DOI, which is determined by model resolution. According to linear approximations, model resolution matrix can be given by (Loke and Barker 1996):

$$\boldsymbol{R} = \left(\boldsymbol{G}^T\boldsymbol{G} + \boldsymbol{C}\right)^{-1}\boldsymbol{G}^T\boldsymbol{G} \tag{3}$$

The model resolution takes values $0 \le R \le 1$, where 1 is perfectly resolved and 0 is unresolved (Wilkinson et al. 2006). The array optimization methods aim to choose array configurations that maximize the values of the resolution matrix. "Compare R" method is an optimization strategy for ERT. It involves determining a limited number of electrode

arrays that maximize the resolution matrix of the models (Loke et al. 2010). The procedure for "Compare R" method is as follows. Step 1: Determining starting base dataset and comprehensive set of arrays. Step 2: Computing the resolution of the base dataset plus new array dataset selected from comprehensive set. Step 3: Ranking resolution, with the first ranked as the new base dataset. Step 4: Repeating steps 2 and 3 until the resolution meets the specified requirement.

For a measurement with X current and potential electrodes, there are $X(X-1)(X-2)(X-3)/8$ array configurations (Xu and Noel 1993). To limit the number of potential configurations, arrays with low stability are excluded. The remaining arrays constitute the "comprehensive" set, and classic arrays set such as Wenner (Fig. S1b) is used as the starting base dataset. The model resolution matrix is recalculated directly upon the addition of a new array to the base dataset. The Sherman-Morrison rank-1 update is utilized for computing the alteration in the resolution matrix following the addition of a single array to the base dataset (Golub and Loan 1989), then the matrices are update as follows (Wilkinson et al. 2006).

$$G^T G \rightarrow G^T G + g \otimes g$$
$$\left(G^T G + C\right)^{-1} \rightarrow \left(G^T G + C\right)^{-1} - \frac{z \otimes z}{1+\mu} \quad (4)$$

where $z = \left(\mathbf{G^T G} + \mathbf{C}\right)^{-1} g, \mu = g \bullet z$ and $a \otimes b$ denotes the matrix multiplication of a and b^T. The vector g is the vector involving sensitivity values of the array. The function, F_{CR}, ranks the refinement in the model resolution resulting from the addition of the array. It is given by:

$$F_{CR} = \frac{1}{k} \sum_{j-1}^{k} \frac{R_{b+1}(j,j)}{R_b(j,j)} \quad (5)$$

where k is the number of model cells. This is used to evaluate the capability of the optimization strategies. R_b is the base dataset model resolution and R_{b+1} is the base dataset plus new array dataset model resolution. In this study, the survey arrays were optimized using this method for 40 iterations and 5263 array configurations were selected (Fig. S1c).

Risk assessment and prediction

The basics of risk assessment are contaminant hazard identification and risk exposure assessment (Sims et al. 2022). Hazard identification requires the information of contaminant types and concentration, land use types, sensitive sites, and persons (Orellana-Macías et al. 2021). The contaminants of interest are confirmed according to the result of environmental investigation and monitoring from boreholes and ERT, which are potential risk to sensitive receivers such as populations. The effects of contaminants on human health and ecology are analyzed through various pathways. Risk exposure situations are those in which contaminants are transported and reach sensitive receivers via different exposure pathways for a given land use type. Risk assessments are divided into pollution degree risk assessment, human health risk assessment, and ecological risk assessment on the basis of receiver features (Fei et al. 2017).

The methods of risk assessment mainly include index-based methods, statistical methods, and GIS-based models (Jain 2023). Index-based methods calculate index or score according to multiple factors such as hydrogeology, human activities, and land use (Goyal et al. 2021). These factors are quantified to several parameters and the index represents the vulnerability of the groundwater environment. Index-based methods are often simple to operate, easy to acquire data, cost-effective, and have been widely used that mainly involve single-factor pollution index (I), Nemerow pollution index (NI), DRASTIC method, GOD method, SINTACS method, et al. However, these methods lack sensitivity to certain contaminants and may not be suitable for all hydrogeological settings (Torkashvand et al. 2021).

In the context of groundwater contamination assessment using statistical methods, the relationship is simulated between one or more independent parameters (e.g., contamination sources, hydrogeological properties, land use) and response variable such as contaminated or not contaminated. The commonly used statistical models for groundwater contamination comprise logistic regression, fuzzy logic, and neural networks. The strengths of these methods lie in managing multiple predictor variables and handling uncertainty and imprecise data, while it needs prior information, as well as the necessity to select appropriate membership functions (Jain 2023).

GIS-based models combine various layers of spatial data for overlay analysis, with each layer reflecting a distinct factor impacting groundwater vulnerability. The results would indicate the degree of groundwater vulnerability to contamination with assigned weight or importance. The contaminant distribution and hydrogeological condition used for risk assessment could be acquired by borehole drilling and ERT. GIS-based models offer advantages in incorporating stakeholder preferences and addressing uncertainty and variability in data. However, they can be complex and time-consuming, requiring extensive data collection and analysis, and may involve subjective judgments and trade-offs between conflicting criteria (Jain 2023).

As an important means of risk assessment, simulation and prediction of contaminants is used to model the flow and transport processes of the aquifer (Egbueri and Agbasi 2022). The conceptual model for simulation and prediction incorporates the hydrogeology and contamination

information refined by integrating hydrochemical, hydrogeological, and ERT method to establish a groundwater flow model (McDonald and Harbaugh 1988).

$$\frac{\partial}{\partial x}\left(k_{xx}\frac{\partial h}{\partial x}\right) + \frac{\partial}{\partial y}\left(k_{yy}\frac{\partial h}{\partial y}\right) + \frac{\partial}{\partial z}\left(k_{zz}\frac{\partial h}{\partial z}\right) + W = S_s\frac{\partial h}{\partial t} \quad (6)$$

where k_{xx}, k_{yy}, and k_{zz} are the hydraulic conductivity along the x, y, and z coordinate axes; h is the hydraulic head; W is the volumetric flux per unit volume representing sources and/or sinks of water; S_s is the specific storage of the porous material; and t is time. The simulation of groundwater flow is conducted and the hydraulic heads are calibrated until the simulation matches the in situ observations. After the groundwater flow model is calibrated, contaminant transport model is established by inputting contaminant source area and concentration values (Zheng and Wang 1999).

$$\frac{\partial(\theta C^k)}{\partial t} = \frac{\partial}{\partial x_i}\left(\theta D_{ij}\frac{\partial C^k}{\partial x_j}\right) - \frac{\partial}{\partial x_i}\left(\theta v_i C^k\right) + q_s C_s^k + \sum R_n \quad (7)$$

where C^k is contaminant concentration of species k; θ is the porosity of the subsurface medium; D_{ij} is the hydrodynamic dispersion coefficient tensor. v_i is the seepage or linear pore water velocity; q_s is the volumetric flow rate per unit volume of aquifer representing fluid sources (positive) and sinks (negative); C_s^k is the concentration of the source or sink flux for the contaminant; $\sum R_n$ is the chemical reaction term. Another calibration is carried out to match contaminant concentrations between simulation and in situ observation. After calibration, the model is capable of predicting the future flow of groundwater and transport of contaminants. The results can be used to help make environmental suggestions and measures.

Case study

In this section, we select a nitrogen-contaminated site to demonstrate the use of the proposed framework. Borehole investigation and ERT survey were conducted to acquire hydrochemical, hydrogeological, and resistivity data. All data were integrated to refine contaminant distribution and hydrogeological condition for risk assessment and prediction. The details of the application are introduced in this section.

Site description

The area of interest is a former fertilizer plant and is still in operation (Fig. 2). It is located in the center of Shandong Province, China, and covers an approximate area of 153,000 m². During the early times of operation, it produces 175,000 t of fertilizer every year, mainly consisting of synthesis ammonia 60,000 t, urea 100,000 t, and methyl alcohol 15,000 t. After 2015, the fertilizer plant changed its products from nitrogenous fertilizer to phthalic anhydride and melamine. An accident reportedly occurred during the operation of the factory, resulting in the leakage of raw materials and products. The potential contaminants are mainly composed of nitrate, nitrite, and ammonia nitrogen compounds, as well

Fig. 2 Satellite image of assessed site. Satellite image of the study area (yellow dashed lines) and residential properties (red dashed lines). Chaiwen river is located to the north of the study area and hilly area is to the south
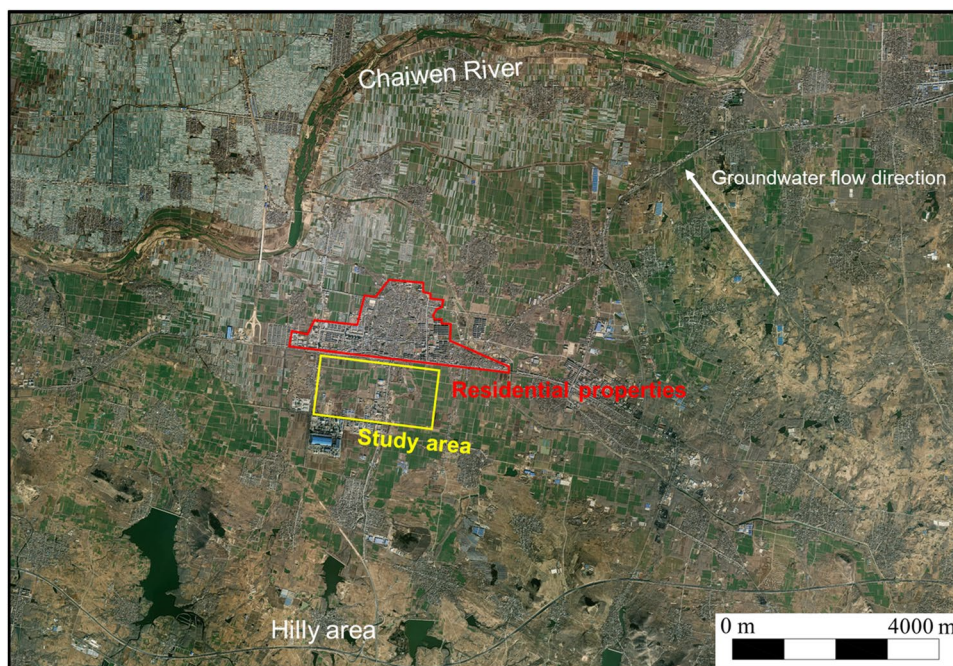
as a small amount of organic matter and metal compounds. Within the plume, the contamination is composed of a high concentration of nitrate, nitrite, and ammonia nitrogen (3-nitrogen).

In addition, local farmers used sewage discharged from the former fertilizer plant to irrigate their crops putting soil compaction. The infiltrated sewage also had the potential to contaminate surrounding groundwater, and crops could even be harmful to human health. Indeed, soil compaction was observed at the surface of the farmland and as deep as 2–3 m below ground surface (bgs). Since a portion of the groundwater was used for domestic purpose, and considering the potential need for emergency water supplies, the residential properties located to the north of the factory are identified as sensitive areas for the groundwater environment protection objectives in this risk assessment.

The geological stratum in this site consists of soil, red stacked stone, and limestone from top to bottom (Fig. S2b). Generally, the thickness of soil layer reaches 5–15 m and the second layer is red stacked stone with a low permeability, which is a regional aquifer mainly distributed to the north of the factory. The thickness of red stacked stone is 2–18 m. The last layer is limestone with an average thickness of

117–130 m. The groundwater of the study area is mainly Quaternary phreatic water and karst water. The average groundwater level is approximately 5–6 m bgs. Groundwater flow direction is from southeast to northwest according to previous hydrogeology survey, and was verified by the interpolation results for groundwater level in monitoring wells (Fig. S2a). The low permeability red stacked stone to the north of the factory may limit the spread of contaminants to sensitive areas. The last limestone layer may also be effective in restricting contaminants transport to confined aquifer.

Groundwater and soil samplings

Borehole survey was carried out to obtain hydrochemical data and verify ERT result. The density of groundwater sampling was approximately one sample per 200×200 m^2 in areas farther from the factory and per 80×80 m^2 closer to the factory. Twenty-one groundwater and thirteen soil samples were collected (Fig. 3). Boreholes and subsequent ERT profiles were densified to the northwestern of the plant because of the groundwater flow direction from southeast to northwest, which can help to delineate the transport of contaminants and explore their influence on sensitive area. The
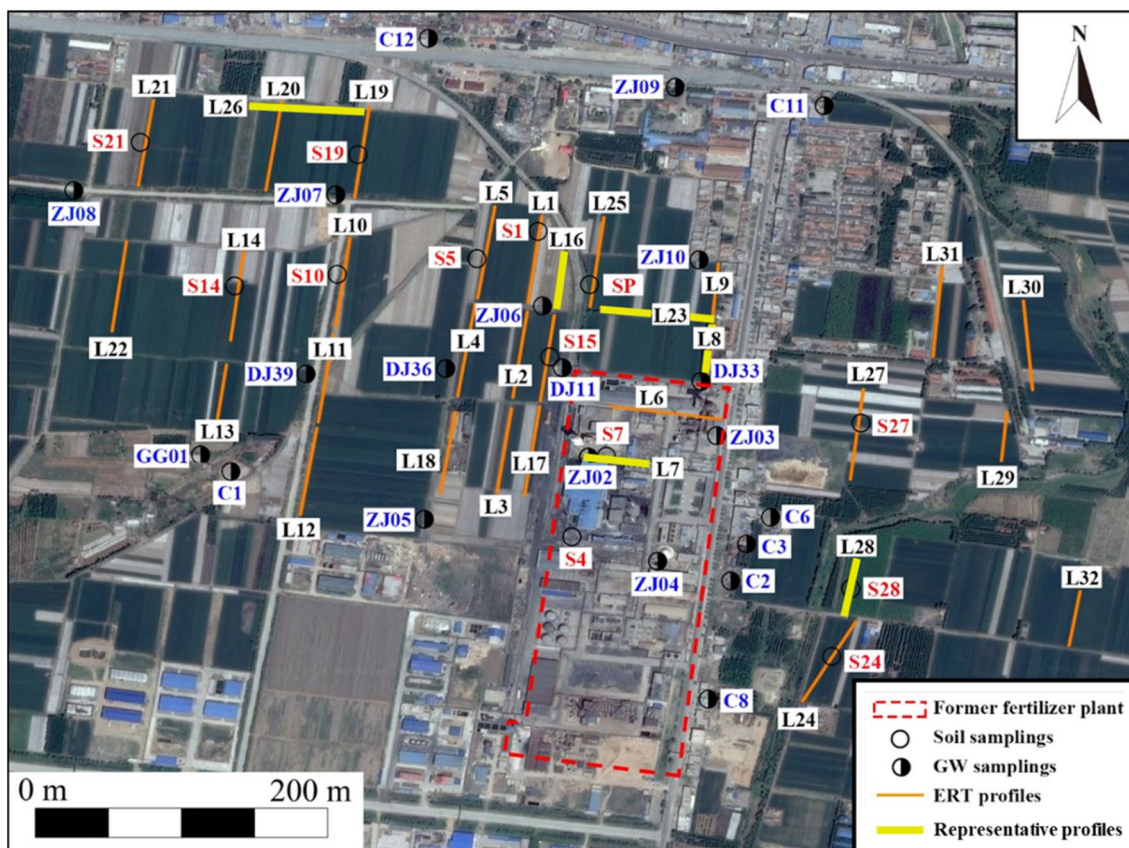
Fig. 3 Deployment of field work. The white and black circles markers represent soil and groundwater samplings locations. A total of 34 ERT profiles are shown by orange lines. Two profiles were arranged inside the plant. Representative ERT profiles are shown by bold yellow lines

groundwater samples were collected using dual-actuator EUI (Solinst 408) and soil samples using direct push technology.

The groundwater samples were tested in situ for factors such as pH, EC, ORP, and DO by a handheld water quality meter (HACH-HQ40d). Besides, the groundwater samples were analyzed in laboratory for K^+, Ca^{2+}, Na^+, Mg^{2+}, SO_4^{2-}, and Cl^- by ion chromatography analysis (Thermofisher ICS-900), CO_3^{2-} and HCO_3^- by the acid–base titration method, and NO_3-N, NO_2-N, NH_4-N, and TN by spectrophotometry (Shimadzu UV-2600). These parameters were utilized to delineate hydrochemical characteristics and evaluate contamination situation, and further infer pollution source to guide control measures. The location and depth of soil samplings were determined by the results of ERT survey. Soil samples were collected at the depth of 2 m bgs above the groundwater level to explore the impact of sewage irrigation on contamination. Representative samples were tested for contaminant index (NO_3-N, NO_2-N, NH_4-N, and TN). Groundwater samples were collected in plastic containers and soil samples were placed in aseptic bags. All samples were stored at 4 °C in iceboxes and promptly transported to the laboratory. All analyses were completed within 10 days.

ERT survey

Geophysical resistivity survey was conducted with the data acquisition in 32 profiles totaling in 4.5 km (Fig. 3). All of them are distributed on the fertilizer plant and in the surroundings and 32 stainless steel electrodes were deployed for current transmission as well as potential measurements, some with an electrode spacing of 3 m (L7, L8, L9, L13, L16, L28, L29, and L32), and others with an electrode spacing of 5 m.

Two profiles (L6 and L7) were present at the plant, and take groundwater flow direction account into; we have laid out several profiles (L8, L9, L23, and L25) to the north to identify the risk to sensitive site. The file shows that different water were used to irrigate crops on both sides of the former fertilizer plant, in which the difference is that the farmland to the east of the plant farmer irrigated crops with water from river and west of the plant they irrigated crops with wastewater discharged from the fertilizer plant. Therefore, we implemented some profiles to analyze different resistivity response.

Resistivity data were collected using ABEM Terrameter LS 2 system and the stacks of measurement were repeated twice and completed in approximately 2 h. Salt solution was infiltrated into the soil around electrode, which can dramatically reduce electrode contact resistance and increase data quality. Additionally, negative apparent resistivity data were excluded during the preprocessing procedure. RES2DINV was used for inversion based on the smoothness-constrained

least-squares method (Loke and Barker 1996). To obtain more accurate results, the cells of inversion model were set to half the electrode space. The depth range was extended by adjusting the factor from 1.05 to 2.

Single-factor pollution index and Nemerow pollution index

Single-factor pollution index (I) is an assessment method for a single factor to reflect the risk of the single contaminant and the assessment indicators are mainly based on national standards:

$$I_i = \frac{C_i}{S_i} \tag{8}$$

where C_i is the concentration of contaminant i in groundwater and S_i is the assessment standard of contaminant i in groundwater. When I_i is > 1, the concentration of that contaminant exceeds the standard. The single-factor pollution index is simple to calculate and can clearly determine the main contaminant factors and contamination areas (Yin et al. 2017). The class III standards in GB/T 14848–2017 were applied in this study, as they are suitable for centralized domestic drinking water supply as well as industrial and agricultural water use.

Nemerow pollution index (NI) is an assessment method for several factors to reflect the mean and maximum values of contaminant indicators based on single-factor pollution index:

$$NI = \left(\frac{\left[(1/n) \sum \left(C_i/S_i \right) \right]^2 + \left[max\left(C_i/S_i \right) \right]^2}{2} \right)^{1/2} \tag{9}$$

where n is the number of factors. The contamination level in groundwater was assessed with NI divided into 6 degrees (Table 1) (Krcmar et al. 2018). The Nemerow pollution index provides a more comprehensive and scientific description of the general state of environmental quality in the assessment area. These indices reveal the groundwater contamination risk at the borehole location, and when

Table 1 Classification of NI (Krcmar et al. 2018)

Class	Pollution degree	NI
0	No pollution	≤ 0.5
1	Clean	0.5–0.7
2	Warm	0.7–1.0
3	Polluted	1.0–2.0
4	Medium pollution	2.0–3.0
5	Severe pollution	> 3.0

combined with ERT results, they can further provide the spatial distribution of groundwater risk.

Prediction of long-term risks of groundwater

The simulation of groundwater flow and contaminant transport was modeled by using the Groundwater Modeling System (GMS). The stratigraphic structure was established in the GMS based on hydrogeological borehole data, and the stratigraphic parameters were set according to the previous field investigation. The stratigraphic boundary was refined combined with ERT results to demonstrate application of the integrating methods. Boundary conditions were set to constant water head at the northern river and zero flux boundary at the southern watershed. Module MODFLOW was used to simulate groundwater flow with the calibration hydraulic heads data came from boreholes. Infiltration of atmospheric precipitation was used as source and equilibrium calibration was performed after the groundwater flow simulation.

The distribution of TN contaminant concentration delineated above was modeled as initial condition and 20 years of simulation were implemented. The effects of convection and diffusion on solute transport are considered in numerical simulation and other factors such as adsorption and biodegradation are neglected to avoid the risk of skewed data during the transportation process. Prediction results for the next 20 years with ERT integration and without ERT integration were shown for comparison.

Results

Hydrochemical results

Table 2 lists the statistical information for groundwater hydrochemical properties in this application based on borehole sampling. The pH values ranged from 6.84 to 9.07 with an average of 7.34 and were slightly alkaline. TDS and total hardness (as $CaCO_3$, TH) were relatively high with the over standard rate of 76.19% and 71.43%, respectively. The range of TDS was mainly 1000–2000 mg/L, which accounted for 66.67% of the samples, followed by 500–1000 mg/L and 2000–3000 mg/L, which accounted for 23.81% and 9.52%, respectively. The area with TDS less than 500 mg/L was mainly concentrated to the east and north of the former fertilizer plant, and the area with high concentration was distributed to northwest and west of the factory; it was consistent with the groundwater flow. High levels of these indicators may result in soil compaction, impacting crop growth, and even posing a risk of kidney stone formation in individuals. It is worth noting that CO_3^{2-} were not detected in all the groundwater samples while HCO_3^- and SO_4^{2-} dominated

**Table 2** Statistical analysis results of hydrochemical data

Index	Minimum	Maximum	Mean	National standard	Over standard rate (%)
pH	6.84	9.07	7.34	6.5 ~ 8.5	9.52
TDS	548	2968	1291.48	1000	76.19
TH	55.2	1092	548.23	450	71.43
K	0.9	24.7	5.5	/	/
Ca	6.2	334	197.22	/	/
Na	27.7	140	68.25	200	0
Mg	8.01	67.5	32.28	/	/
CO_3	/	/	/	/	/
HCO_3	354.2	8116	967	/	/
SO_4	75.3	1010	288.67	250	42.86
Cl	50.6	348	120.20	250	4.76

Units for all indices are mg/L except pH

the groundwater anions in the study area, and SO_4^{2-} with a high over standard rate of 42.86%.

The concentration distribution of TN is shown in Fig. 4. The range of TN concentration was from 29.1 to 615 mg/L, with an average concentration of 120.38 mg/L. Among the 21 groundwater samples, 5 samples had TN concentration less than 50 mg/L, 7 samples had a range of 50 ~ 100 mg/L, and 9 samples had concentration greater than 100 mg/L. Areas with high concentration (> 100 mg/L) were mainly distributed inside the plant. Along the groundwater flow direction, the TN concentration decreased gradually. Because of high concentrations of TN, the factory relied on an industrial water supply sourced from a confined aquifer with well depths reaching up to 200 m.

Table 3 shows the statistical analysis of groundwater nitrogen content. NO_3-N, NO_2-N, and NH_4-N were detected in all samples and the main forms of nitrogen contaminants were NH_4-N and NO_3-N, with over standard rate of 90.84% and 85.71%, respectively. The NH_4-N concentration ranged between 0.103 and 525 mg/L with an average concentration of 45.75 mg/L, which exceeded the maximum acceptable limit (0.5 mg/L) based on the *Standard for Groundwater Quality*. The NO_3-N concentration ranged between 16.2 and 244 mg/L with an average concentration of 55.7 mg/L, which also exceeded the maximum acceptable limit (20 mg/L). In contrast, NO_2-N concentration is much lower with the average of 0.19 mg/L and the over standard rate of 5%. Hence, NH_4-N and NO_3-N are the dominant inorganic N species around the plant. The highest NH_4-N concentration is located in ZJ02 (525 mg/L), where in the fertilizer plant and used for stacking sludge. Meanwhile, the concentration of NH_4-N and NO_3-N distribution has the same characteristics with
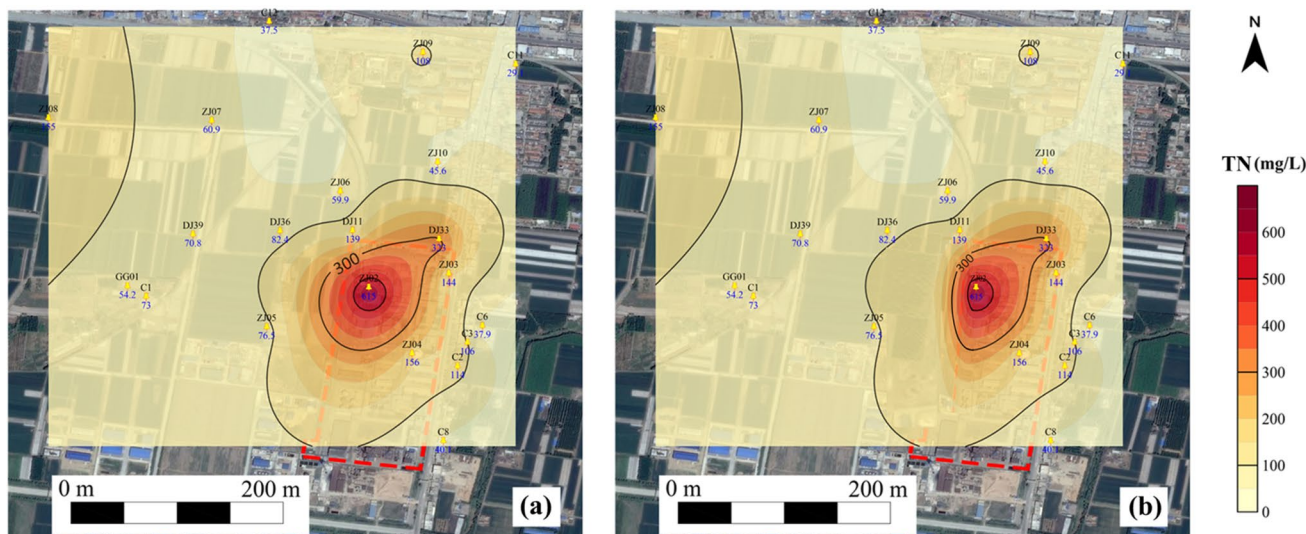
Fig. 4 Distribution of TN contaminants from borehole sampling refined without ERT (**a**) and with ERT (**b**). The study area was severely polluted by nitrogen with non-source contamination and a high concentration source contamination in the north of plant. The area of high concentration contaminants was restricted to a smaller extent at the west boundary of plant

TN concentration distribution. Based on the above analysis, it is clear that the high concentrations of groundwater contaminants have posed a potential threat to the quality of this crucial water resource. These contaminants may migrate into the soil, affecting agricultural produce and posing a risk of exposure to harmful substances during agricultural activities.

Resistivity distribution

The resistivity distribution derived from inversions of ERT data are presented (Fig. 5). Representative examples of resistivity profiles are shown, which include the area under fertilizer plant and potentially contaminated area. When groundwater is contaminated with 3-nitrogen pollutants, groundwater conductivity rises with increasing ion concentrations, leading to a decrease in the resistivity of subsurface medium. Thus, the subsurface below the area of accident taken place was characterized by low resistivity possibly influenced by contaminants emanating from the raw material storage site (L7). The maximum depth

Table 3 Groundwater nitrogen (N) content collected from the study area (mg/L)

Index	Minimum	Maximum	Mean	Over standard rate	
				Standard	Proportion (%)
NO_3-N	16.2	244	55.7	20	85.71
NO_2-N	0.004	1.72	0.19	1	5
NH_4-N	0.103	525	45.75	0.5	90.84

penetrated was 15 m with resistivity values of suspectedly contaminated layers below 16 Ω·m except few isolated areas of high resistivity in the top layer. The high resistivity layer in the first 2 m may be caused by the accumulation of construction wastes originally demolished and the hardening of surface; another profile under the plant (L6) has the same phenomenon.

Profile L8 was located to the north of plant where the resistivity gradually increases from south to north. The groundwater sampled in DJ33 had the highest TDS where resistivity response was similar to profiles under the plant. Profile L23 is about 100 m away from the north boundary of plant with a visible high resistivity response in both top and bottom. The east of the profile had a low resistivity area that is consistent with the north result of L8. Profile L16 is 5 m away from the west boundary of plant and result shows that the south of the profile had low resistivity response consistent with L15. Profile L26 is about 800 m away from plant and the low resistivity area near surface was maybe caused by the river water infiltration in north of the profile. Profile L28 is located to the east of plant and the resistivity result can be divided into three layers. The first layer was about 6 m thick with the resistivity of about 16 Ω·m caused by farm perennial irrigation. The second layer of 6–15 m thickness displayed the resistivity between 30 and 100 Ω·m. The third layer had a rather uniform resistivity higher than 100 Ω·m. These resistivity results show a good agreement with borehole data with the surface layer corresponding to the soil layer and the deep layer corresponding to the limestone layer. In general, profiles with low resistivity are predominantly distributed in

Fig. 5 Representative resistivity profile results. Profile L7 inside the plant indicate significantly low resistivity anomaly caused by the existence of high concentration of contaminants. Profiles L8 and L23 to the north of plant show contaminants transported 50–100 m to the north. The northwest of the study area was not affected by the transport of contaminants based on the result of L16. Profiles L26 and L28 show the resistivity responses of red stacked stone and soil layer, respectively

the contaminated area according to the TN distribution pattern (Fig. 4). The borehole hydrochemical data provide accurate contamination information, while the ERT results reveal a high-resolution distribution of anomalous areas.

The contamination extent was estimated by mapping 3-D resistivity results around the plant from 2-D ERT profiles based on the resistivity value < 16 Ω·m (Fig. 6). Strong contrast between the plant and surrounding area was displayed. The depth range of 0–15 m was marked out as contaminated area. Thus, the low resistivity areas can be used as target for risk management or remediation efforts. According to

drilling information and ERT results, the presence of low-permeability red stacked stone with high resistivity prevented the diffusion of contaminants to the north of the plant. In the future, ERT profiles and monitoring wells could be increased to the north of the plant to jointly monitor the spread of groundwater contamination.

Risk assessment

Pollution degree risk assessment was conducted using single-factor pollution index and Nemerow pollution index

Fig. 6 Three-dimensional resistivity illustration of the study area. Low resistivity anomalies are clearly seen in the north of the plant and had a tendency to transport northward, while transporting a shorter distance westward. The geologic boundary between red stacked stone and soil layer was also distinctly delineated
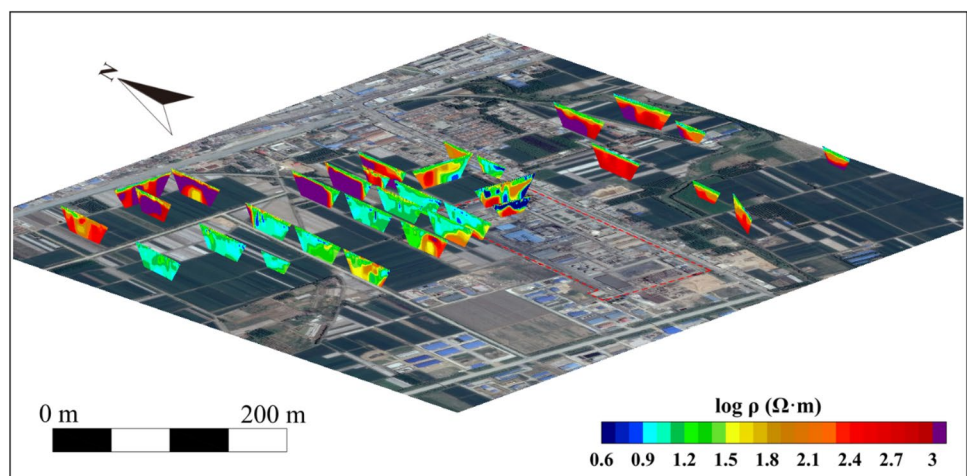
Fig. 7 Single-factor pollution indices (**a**) and Nemerow pollution indices (**b**) of groundwater samples. **a** The black line is used to determine if the pollution concentration exceeds the standard. **b** Above the black, orange, and red lines represent polluted, medium pollution, and severe pollution. All samples were polluted and more than half were severe pollution with NH$_4$-N and NO$_3$-N as the main contaminants
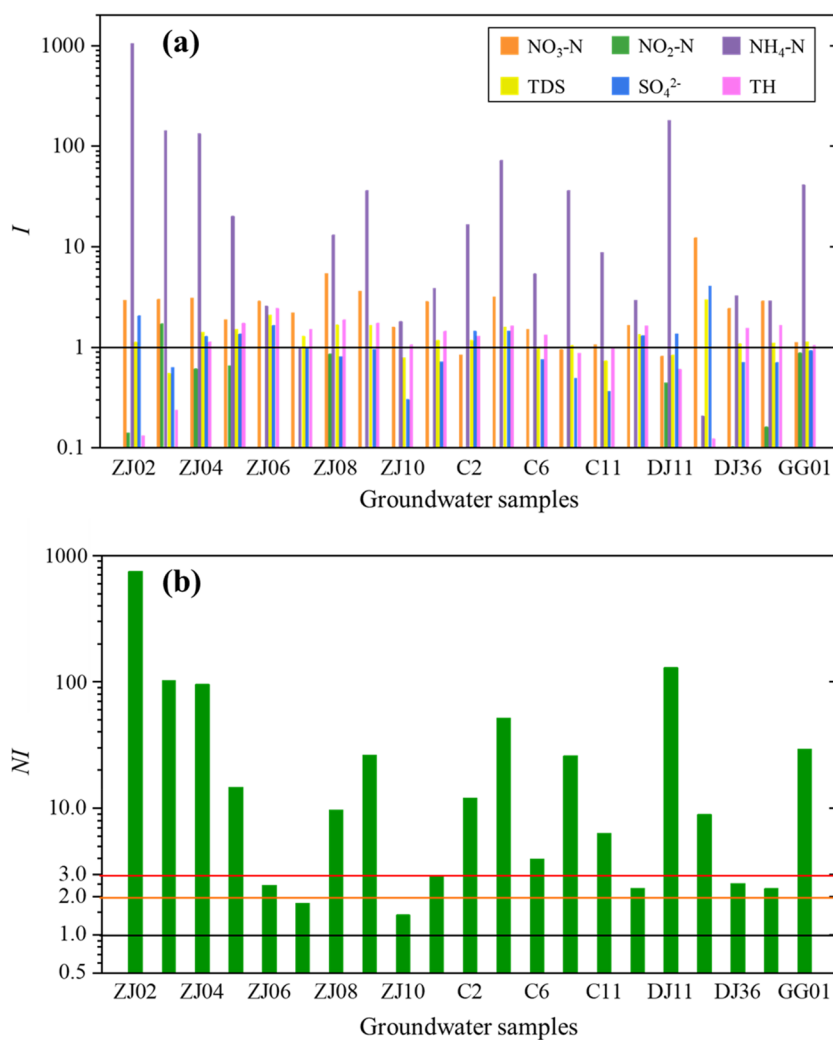
based on six contamination factors over standard (Fig. 7). Single-factor pollution index shows that all the samples exceeded the standard of variable factors. NH$_4$-N was the most severe contamination factor with 19 samples over standard in all 21 samples, followed by NO$_3$-N with 18 samples. The values of I were extremely high for NH$_4$-N with 11 samples over 10, even reaching to 1000. And NO$_3$-N had the next highest value with 12 samples over 2. The pollution degrees of TDS, SO$_4^{2-}$, and TH were similar with almost all I below 2. The most toxic NO$_2$-N was the least pollution degree with only the sample of ZJ03 having I of 1.72 above 1.

NI reflects the combined pollution degree of six factors above, and all the groundwater samples were polluted according to the classification (Table 1). Among these, five samples were classified as medium pollution and 14 samples were classified as severe pollution, which highlight the seriousness of groundwater contamination here. It is worth noting that the most contaminated samples ($NI > 100$) were all from boreholes inside or near the

plant consistent with ERT results. Thus, the ERT results can help to identify the high-risk areas ($NI > 100$) by the low resistivity responses (< 16 Ω·m). Combined I and NI results, while regional groundwater is heavily contaminated, the most prominent factors are NO$_3$-N and NH$_4$-N. To address the high risk of groundwater contamination, it is recommended to implement measures to control the source of irrigation water and employ groundwater pump-and-treat for remediating high concentration areas below the plant.

The distribution of TN concentration was visualized by interpolation for analyzing the spatial characteristic of dominant contaminants (Fig. 4). The heavily contaminated area was improved with the help of n the established relationships between groundwater conductivity and contaminant concentration (Fig. 4b). The results show that TN was mainly distributed in the north of the plant, with a tendency to diffuse northward and westward consistent with the groundwater flow direction. In addition, patchy contamination is present in ZJ08 and ZJ09 on the northwest

of the study area. With the exception of point source pollution, the study area as a whole had significant nonpoint source pollution. TN concentrations exceeded the standard throughout the region. These contaminations may potentially affect the safety of drinking water and food safety of agricultural products for neighboring residents.

Simulation and prediction of TN contamination

Groundwater head results show that the flow direction was from southeast to northwest in dynamic steady state equilibrium, which is consistent with hydrogeological survey. The maximum water head appeared in zero flux boundary of southern watershed and minimum water head appeared in constant water head of northern river. The hydrogeological parameters were adjusted based on ERT results and the relation between computed and observed groundwater head is shown in Fig. 8b. The $R^2 = 0.965$ indicates a good agreement between simulation results and the groundwater head presented in the borehole survey. In addition, groundwater budget calibration shows the good agreement between total inflows and outflows with the error of 0.0077%.

The TN contamination transport was simulated by using the refined hydrogeological condition and contamination distribution with ERT results. The geologic boundary between the red stacked stone and soil layers was adjusted based on high resistivity (> 100 Ω·m) areas. Meanwhile, heavy contaminated areas were minimized at the western boundary of the plant according to low resistivity (< 16 Ω·m) anomalies. The distribution of groundwater TN contamination plume after 20 years are shown in Fig. 9b. The simulation results indicate a significant transport of the pollution plume towards the northwest influenced by regional hydrogeological conditions with mountains to the southeast and rivers to the northwest. The transport distance differs

with approximately 130 m towards the west and only around 45 m towards the north. Thus, the presence of low permeability red stacked stone in the north limits the diffusion of contaminants to reach environmental sensitive areas of residential properties. However, the farmland to the west of the plant will be affected by heavily contaminated groundwater. Simultaneously, there should be a reduction in the use of fertilizers and pesticides on agricultural land, along with strengthened management of wastewater discharges from industrial areas. These measures aim to mitigate the threat posed by contaminants to human health.

Discussion

Relationship of conductivity and ion concentrations

The relationship between resistivity from ERT survey and groundwater conductivity can be established based on Archie's law (Archie 1942). Therefore, the key for this application is to establish the relationship between groundwater conductivity and contamination concentration. Conductivity is directly proportional to the total ion concentration (Revil and Glover 1997), making the identification of dominant ions in groundwater valuable for achieving the purpose. The major ions in groundwater, including K^+, Ca^{2+}, Na^+, Mg^{2+}, Cl^-, SO_4^{2-}, CO_3^{2-}, and HCO_3^-, primarily determine the groundwater chemical types. Figure 10 can directly reflect the relative content and distribution characteristics of major ions in groundwater.

The dominant cation type was mainly Ca^{2+}, followed by Na^+ and Mg^{2+}, which account for 65.04%, 22.51%, and 10.65% of the samples, respectively. Meanwhile, the dominant type of anion was HCO_3^-, followed by SO_4^{2-}, which accounts for 67.56% and 20.17% of the main anion,
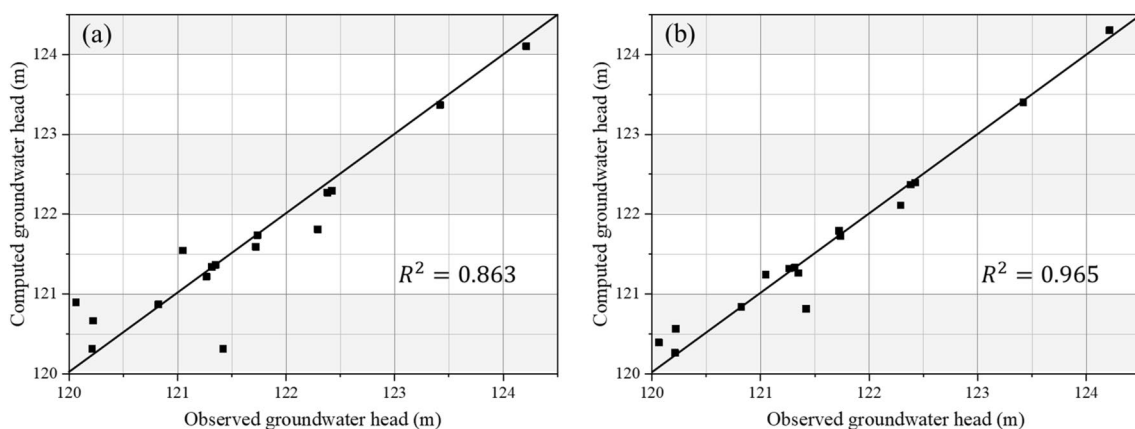

Fig. 8 Comparison of the groundwater head computed by the model and measured in the observation wells. **a** Simulation based on the hydrogeological modeling without ERT constraint. **b** Simulation based on the hydrogeological modeling with ERT constraint. The simulation refined by ERT had a better fitting effect with the R^2 of 0.965

Fig. 9 Prediction results of TN contaminants after 20 years refined without ERT (**a**) and with ERT (**b**). The pollution plume will transport towards the northwest, with spreading farther west than north. The refined result indicates a smaller extent compared to the non-refined result
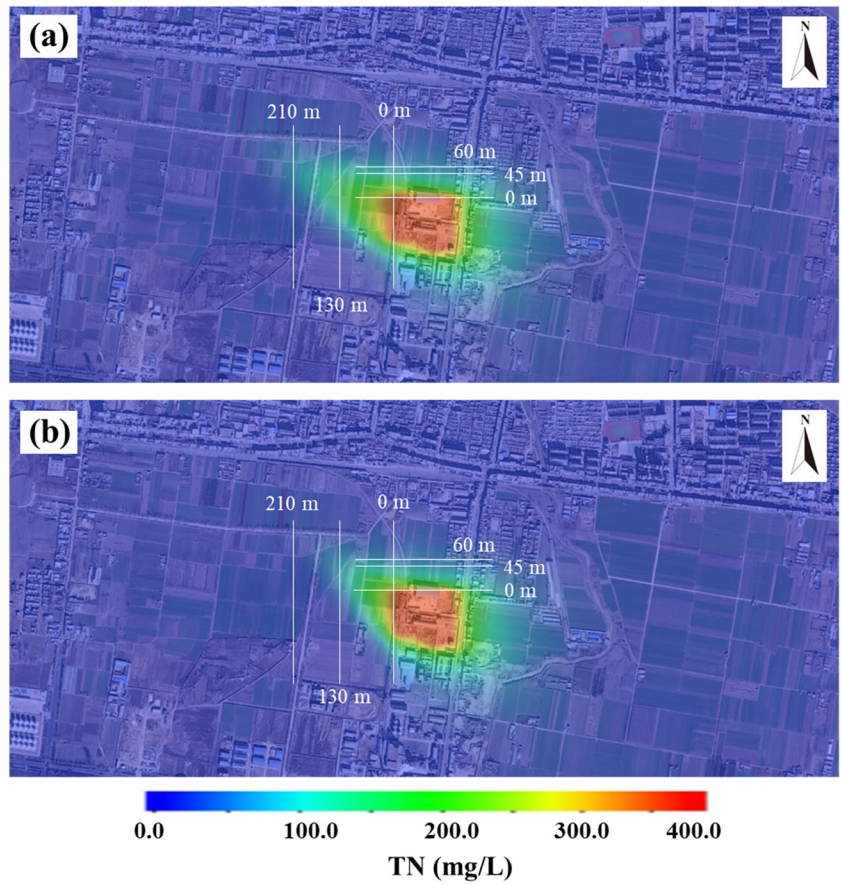
Fig. 10 Piper diagram of groundwater samples. The groundwater types in this area are mainly HCO_3-Ca and SO_4-Ca
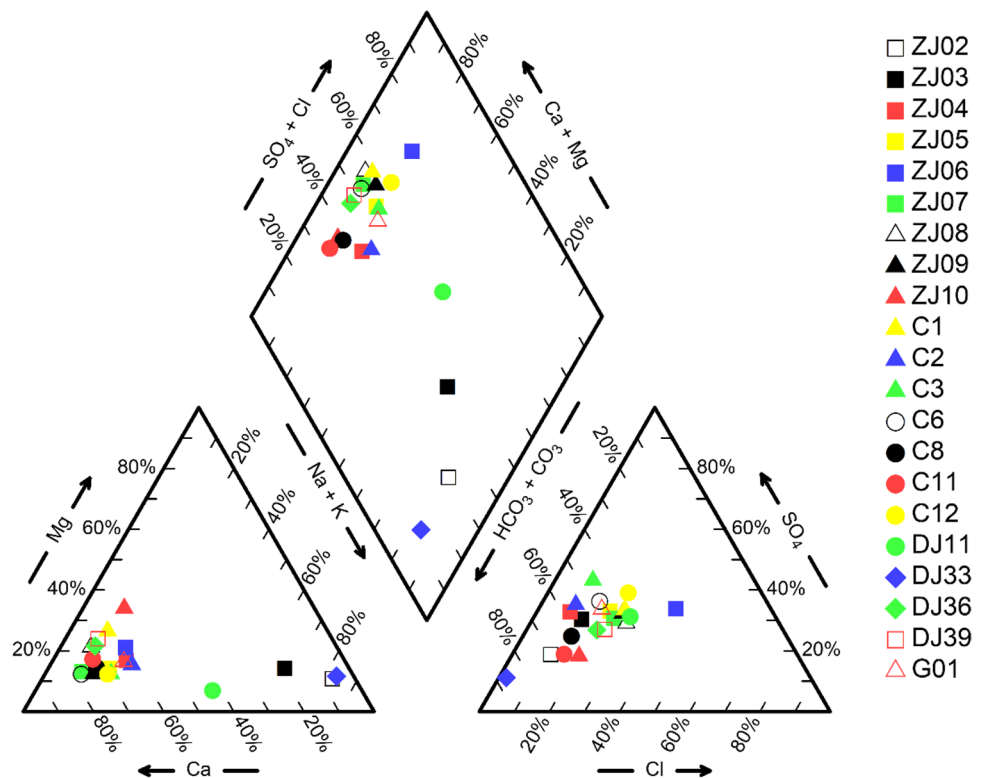
respectively. As can be seen from the Piper diagram, the groundwater types in this area are mainly HCO_3-Ca and SO_4-Ca. Ca^{2+} and SO_4^{2-} ions, potential components of fertilizers, may infiltrate groundwater due to spills from fertilizer plant accidents or as a result of fertilizer application in agricultural activities. The presence of fertilizers can also result in the loss of Ca^{2+} ions. In addition, the decomposition of nitrogen fertilizers may be accompanied by an acidic reaction that releases HCO_3^- ions. Contaminant factor SO_4^{2-} was chosen to analyze the relationship with conductivity in conjunction with the groundwater quality standards. In addition, among the two dominant contaminants above, NH_4-N had a high coefficient of variation and could not be easily related to conductivity. NO_3-N exhibited a small coefficient of variation and shared the same trend as conductivity difference, and can reflect the contamination distribution to some extent. Thus, NO_3-N was selected as another factor to establish the relationship with conductivity.
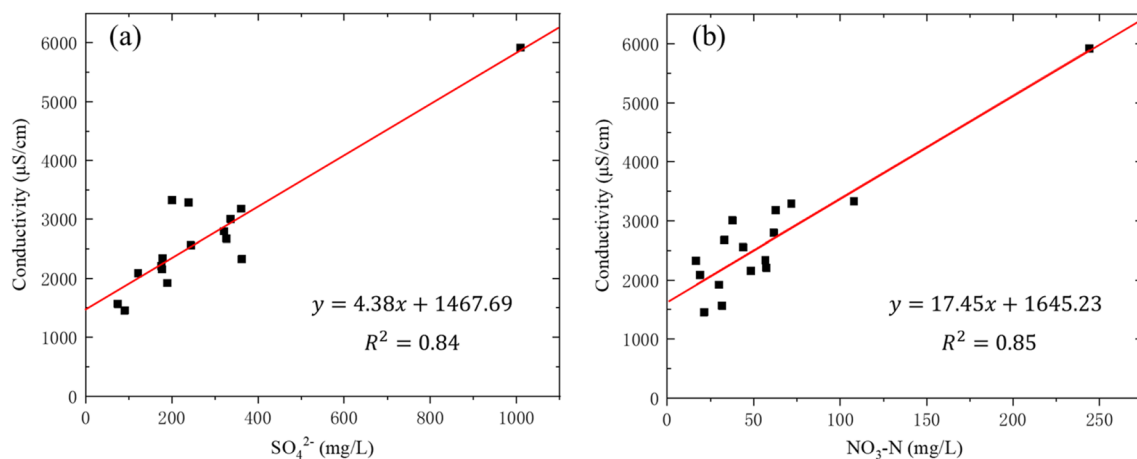
The relationship between the SO_4^{2-} and NO_3-N concentrations and conductivity are shown in Fig. 11. There is a linear correlation between the two ion concentrations and conductivity with coefficient of determination of 0.84 and 0.85. Therefore, ERT results can be used as a basis for delineating the extent and degree of SO_4^{2-} and NO_3-N contamination. According to the Archie's law, the interconnected porosity and cementation exponent of subsurface medium can be measured and calculated by laboratory experiment for soil and groundwater samples (Glover 2009). Another optional method is to calibrate by borehole sampling at the same locations of ERT survey lines and obtain the integration of interconnected porosity and cementation exponent based on the resistivity of field ERT results and the conductivity of groundwater (McCall and Christy 2020). After the two parameters have been determined, the conductivity distribution of groundwater can be characterized from the ERT profiles. The conductivity distribution of groundwater is then calculated to contaminant distribution based on the established relationship between conductivity and contaminant concentration. In addition, resistivity thresholds for contamination classification can also be determined based on groundwater quality standards. The primary methodology employed for the aforementioned studies involved regression analysis between subsurface medium resistivity, groundwater conductivity, and contamination concentrations. The accuracy relies on the coefficient of determination derived from the regression analysis.

Delineation and prediction of contamination constrained with ERT

Traditional characterization and monitoring methods for groundwater contamination typically rely on data from sparse, vertically oriented boreholes. Geophysics methods such as ERT can be used to obtain continuous information between boreholes. Although ERT is a mature method, to data most field application of ERT for characterization and monitoring of different sites is well known that the imaging resolution obtained from ERT using surface electrodes decreases with depth (Wilkinson et al. 2006). It is an especially important consideration for some area that contamination plume has penetrated to a large depth.

An optimized method for field resistivity acquisition array is necessary. Here, we considered the application of the optimized array method for field data acquisition (Loke et al. 2010). The results proved that the CR method can significantly improve the resolution of ERT compared to conventional arrays. From the inversion results of resistivity collected from this site, we found that the detection depth of optimized array reaches to one-third of the length of measurement line, which is a significant improvement over

Fig. 11 Relationship between conductivity and SO_4^{2-} (**a**) and NO_3-N (**b**) contaminant concentrations. The main contaminants and conductivity show a good agreement with R^2 of 0.84 and 0.85, respectively

traditional arrays with one-sixth to one-fifth, such as gradient, dipole–dipole, and Wenner array (Meng et al. 2022a).

The TN concentration from borehole sampling was interpolated to delineate the distribution of contaminants for risk assessment and numerical simulation (Fig. 4a). ERT results were integrated to refine the interpolation result by constrain the heavily contaminated area at the west boundary of plant (Fig. 4b). The ERT profiles L2, L3, L15, and L17 were applied in the integration procedure. The comparison indicates that the results constrained without ERT had a larger diffusion of contaminants at the western boundary of the plant, while the results constrained with ERT limit the extent of heavily contaminated area. The overestimation of contaminated areas constrained without ERT derived from the lack of inter-borehole information generated by sparse boreholes, while the application of ERT filled this gap. The accurate characterization results based on ERT survey resulted in more reliable risk assessment and prediction, and will reduce the cost of subsequent risk management and remediation of groundwater contamination.

In addition to delineating contamination distribution, the demarcation of the boundary between the red stacked stone layer and the soil layer in the north of the study aera was also optimized using ERT results. Both optimization results were applied to the construction of the numerical model for groundwater flow and contaminant transport. The calibration between simulated and observed groundwater head was implemented by the borehole head data (Fig. 8). The results integrated without ERT show a good agreement with R^2 of 0.863, while the results with ERT indicate a better agreement with R^2 of 0.965. Thus, the simulation results integrated with ERT are more reliable because of the refinedly hydrogeological parameters.

Simulation results integrated with ERT and without ERT are shown in Fig. 9. The refined result indicates a smaller extent after 20 years with the heavily contaminated area (> 100 mg/L) of 48,232 m^2 compared to the non-refined result of 63,241 m^2. The non-refined results had a westward transport distance of 210 m, while the refined result had only 130 m, with a northward distance of 60 m and 45 m, respectively. The limited westward transport distance was mainly contributed to the improvement of contamination distribution and northward distance was the refinement of hydrogeological parameters. Thus, the integration of hydrochemical data and ERT method for correcting contamination distribution and hydrogeological conditions resulted in the more reliable prediction.

The application of refined results from ERT in risk management and remediation can reduce time and financial costs. The real-time monitoring capabilities of ERT enable timely adjustments to strategies during remediation, contributing to the overall cost-effectiveness of the remediation process. It is worth noting that the relationship between ERT data and contaminant concentrations in groundwater can be influenced by various factors, including geologic properties and hydrochemical characteristics. They may lead to uncertainty in modeling results of prediction. Indeed, ERT exhibits heightened sensitivity to variations in pore water, particularly inorganic contaminants. Additional pollutants such as organic substances can be delineated in tandem with geophysical methods sensitive to interfaces, such as induced polarization (IP) and ground-penetrating radar (GPR).

Sources of groundwater contamination

The results of risk assessment and numerical simulation indicate that the groundwater environment in study area was heavily contaminated by nitrogen with non-source contamination and a high concentration source contamination. All of nitrogen contaminants were mainly concentrated in fertilizer plant and the accident of plant was potentially viewed as a point source pollution, then spread to other areas. The leakage from the plant gathered and formed non-source pollution with the groundwater flow the agricultural fertilization.

The high nitrate concentration could be attributed to human activities, especially the extensive application of nitrogenous fertilizers in farmlands and the discharge of domestic sewage (Zhai et al. 2017). In the north of the fertilizer plant, groundwater was contaminated by the sludge used to produce fertilizer. On the other hand, sewage was discharged and flowed under the topography. Some farmlands to the west and northwest of the study area also have abnormally nitrogen pollution, and the main cause was frequent agricultural activities. In the north of the study area, some population cluster area has been contaminated by septic tank leakage. Fortunately, there exist low-permeability red stacked stone that has blocked the spread of the contaminants. The red stacked stone may result in contaminants being retained in this region. A targeted remediation strategy could be considered to apply remediation efforts more intensively to the area around the red stacked stone. The NO_2-N pollution in groundwater was relatively light, only 5% over the standard limit. It is worth noting that the irrigation water samples have the second highest concentration with 0.878 mg/L, and the highest concentration located in farmland (ZJ03, 1.72 mg/L) instead of plant. Thus, groundwater NO_2-N pollution was greatly affected by agricultural fertilization or irrigation well.

In addition, ERT survey shows that inversion results of the east and west of the fertilizer plant are different. The resistivity to the west is lower than east at the same depth, and the resistivity inversion results to the east are more structured. In the process of taking soil samples, we found that the soil to the east of the plant is denser than the west. On the other hand, we analyzed that the use of different irrigation water sources is one of the reasons for the difference

Table 4 Soil samples pH and nitrogen contents obtained from the study area

Borehole	pH	NO_3-N	NH_4-N	TN
S1	7.32	1.1	0.46	96.2
S5	7.01	1.79	0.23	111
S10	7.63	5.39	/	276
S14	8.22	8.16	/	175
S15	8.13	2.29	0.16	269
S19	8.13	0.86	0.21	143
S21	8.16	2.23	0.23	277
S24	8.01	4.37	0.44	170.9
S27	7.93	5.44	0.23	174
S28	7.94	2.25	0.23	227.9
SP	7.43	21.09	1.41	352
S7	8.59	36.17	0.17	274.42
S4	8.76	28.44	0.12	117.19
Minimum	7.01	0.86	/	96.2
Maximum	8.76	36.17	1.41	352
Average	7.94	9.20	0.35	204.89

Units for all indices are mg/kg except pH

in resistivity results. Irrigation water to the east is river water and groundwater to the west.

Soil samples were analyzed and the results are shown in Table 4. NO_2-N was not detected in all soil samples. The NO_3-N concentration range from 0.86 to 36.17 mg/kg, with an average concentration of 9.20 mg/kg. However, the NH_4-N concentration was relatively low in soil with the highest concentration of 1.41 mg/kg. The contrast between NO_3-N and NH_4-N contaminants is reversed in groundwater and soil, which further proves that NO_3-N contamination is partly from agricultural fertilization and NH_4-N contaminants are from accident of plant. In addition, the high concentration of NO_3-N in the soil may be attributed to higher oxygen levels promoting the dominance of nitrification, in which ammonia nitrogen is oxidized to nitrate. NO_3-N may be adsorbed, transformed, or trapped during groundwater transport, thus influencing its capability to infiltrate groundwater. However, relevant historical information that may include past industrial activities, waste disposal areas, or underground pipeline leaks may be incomplete or difficult to obtain. This increases the limitations and uncertainties of source identification. Multiple sources of contamination may be present in the groundwater system and this mixing may lead to interactions between different contaminants, making it more difficult to accurately locate the single source.

Suitable environmental measures are needed to protect the soil and groundwater from being contaminated. The anti-seepage measures are necessary for the prevention and removal of the contamination source (Liu et al. 2019). The major control areas must include the residential properties to the north of the plant, as well as the wells for irrigation and domestic use. In the meantime, wells must be designed for monitoring the groundwater system and for the protection of residential areas and water source. The wells need be arranged to enhance monitoring in major contamination control regions and the location can be adjusted according to the contamination source and groundwater flow direction. In addition, ERT will be monitored annually to delineate the spatial variability of heavily contaminated area.

Conclusions

In this study, we developed a general framework for risk assessment of groundwater contamination. Both borehole investigation and ERT survey are integrated in our framework. The preliminary information of target area is collected and borehole drillings are conducted to identify contamination concentration. The ERT survey is subsequently implemented after defining the data acquisition strategy and optimizing the array. Inversion results are integrated to refine contamination distribution and hydrogeological condition. The refined contamination and hydrogeology information are used for risk assessment and prediction of contaminants. Finally, suggestions and measures are proposed based on the refined risk assessment and prediction for groundwater protection. Compared to traditional borehole-based techniques, this framework enables risk assessment through the sequential integration of hydrochemical, hydrogeological, and ERT surveys by establishing petrophysical relationships among these datasets.

A nitrogen-contaminated site was assessed to demonstrate the use of the framework. The results show that the ERT results were in good agreement with hydrochemical data and the relationship between contaminant concentrations and conductivity were established for data integration with $R^2 > 0.84$. Contamination distribution interpolated by borehole data was significantly improved by ERT constraint. Numerical simulation was developed using the refined contamination data. Comparison results show that the calibration of ERT-based numerical model had a better coefficient of determination 0.965 between computed and observed groundwater head. Therefore, it is more reliable to integrate ERT results for correcting contamination distribution in numerical modeling, enhancing the accuracy and cost-effectiveness of subsequent contamination transport predictions and remediation efforts.

Risk assessment results show that the study area was severely polluted by nitrogen with non-source contamination and a high concentration source contamination in the north of the chemical plant, especially NH_4-N and NO_3-N. Contaminant NH_4-N was primarily distributed in groundwater through leakage from the plant accident and NO_3-N had

a similar distribution in groundwater and soil due to agricultural fertilization. Prediction indicate that high concentration will transport northwest and has an influence area of 48,232 m^2, which will not affect the residential properties nearby. Optimizing the arrangement of monitoring wells based on contamination spread prediction to ensure coverage of potential pathways can help improve the efficiency of monitoring. At the same time, groundwater management policies can help to optimize source control measures, potentially including limitations on fertilizer use or regulation of industrial discharges. In this study, ERT was integrated but uncertainties still exist in the data fusion process. Future research could be devoted to the development of multi-source mixing models to better simulate the complex transport pathways.

Declarations

Ethics approval All analyses are based on publicly available data and therefore do not require ethical approval.

Consent to participate All authors gave their consent to participate in this study.

Consent for publication All authors approved the final manuscript and the submission to this journal.

Competing interests The authors declare no competing interests.

References

Akiang FB, Emujakporue GO, Nwosu LI (2023) Leachate delineation and aquifer vulnerability assessment using geo-electric imaging in a major dumpsite around Calabar Flank Southern Nigeria. Environ Monit Assess 195(1):123

Archie GE (1942) The electrical resistivity log as an aid in determining some reservoir characteristics. Trans Am Inst Min Metall Pet Eng 146:54–62

Balasco M, Lapenna V, Rizzo E, Telesca L (2022) Deep electrical resistivity tomography for geophysical investigations: the state of the art and future directions. Geosciences 12(12):438

Binley A, Slater L (2020) Resistivity and induced polarization: theory and applications to the near-surface Earth. Cambridge University Press, Cambridge

Calò F, Parise M (2009) Waste management and problems of groundwater pollution in karst environments in the context of a post-conflict scenario: the case of Mostar (Bosnia Herzegovina). Habitat Int 33(1):63–72

Chu Y, Liu S, Wang F, Cai G, Bian H (2017) Estimation of heavy metal-contaminated soils' mechanical characteristics using electrical resistivity. Environ Sci Pollut R 24(15):13561–13575

de Barros FPJ, Bellin A, Cvetkovic V, Dagan G, Fiori A (2016) Aquifer heterogeneity controls on adverse human health effects and the concept of the hazard attenuation factor. Water Resour Res 52(8):5911–5922

Egbueri JC, Agbasi JC (2022) Data-driven soft computing modeling of groundwater quality parameters in southeast Nigeria: comparing the performances of different algorithms. Environ Sci Pollut R 29(25):38346–38373

Fei JC, Min XB, Wang ZX, Pang ZH, Liang YJ, Ke Y (2017) Health and ecological risk assessment of heavy metals pollution in an antimony mining region: a case study from South China. Environ Sci Pollut R 24(35):27573–27586

Flores-Orozco A, Gallistl J, Steiner M, Brandstätter C, Fellner J (2020) Mapping biogeochemically active zones in landfills with induced polarization imaging: the Heferlbach landfill. Waste Manage 107:121–132

Fu HY, Ding DX, Sui Y, Zhang H, Hu N, Li F, Dai ZR, Li GY, Ye YJ, Wang YD (2019) Transport of uranium(VI) in red soil in South China: influence of initial pH and carbonate concentration. Environ Sci Pollut R 26(36):37125–37136

Glover PWJ (2009) What is the cementation exponent? A new interpretation. Leading Edge 28:82–85

Golub GH, Loan CFV (1989) Matrix computations (2nd edn). Johns Hopkins University Press

Goyal D, Haritash AK, Singh SK (2021) A comprehensive review of groundwater vulnerability assessment using index-based, modelling, and coupling methods. J Environ Manag 296:113161

Han DM, Currell MJ, Cao GL (2016) Deep challenges for China's war on water pollution. Environ Pollut 218:1222–1233

Hou D, Al-Tabbaa A, O'Connor D, Hu Q, Zhu YG, Wang L, Kirkwood N, Ok YS, Tsang DCW, Bolan NS, Rinklebe J (2023) Sustainable remediation and redevelopment of brownfield sites. Nat Eev Earth Env 4(4):271–286

Jain H (2023) Groundwater vulnerability and risk mitigation: a comprehensive review of the techniques and applications. Groundw Sustain Dev 22:100968

Karunanidhi D, Aravinthasamy P, Subramani T, Kumar D, Venkatesan G (2021) Chromium contamination in groundwater and Sobol sensitivity model based human health risk evaluation from leather tanning industrial region of South India. Environ Res 199:111238

Krcmar D, Tenodi S, Grba N, Kerkez D, Watson M, Roncevic S, Dalmacija B (2018) Preremedial assessment of themunicipal landfill pollution impact on soil and shallow groundwater in Subotica, Serbia. Sci Total Environ 615:1341–1354

Kumar P, Tiwari P, Biswas A, Acharya T (2023) Geophysical investigation for seawater intrusion in the high-quality coastal aquifers of India: a review. Environ Sci Pollut R 30(4):9127–9163

Lawniczak AE, Zbierska J, Nowak B, Achtenberg K, Grzeskowiak A, Kanas K (2016) Impact of agriculture and land use on nitrate contamination in groundwater and running waters in central-west Poland. Environ Monit Assess 188(3):172

Li P, Tian R, Xue C, Wu J (2017) Progress, opportunities, and key fields for groundwater quality research under the impacts of human activities in China with a special focus on western China. Environ Sci Pollut Res 24(15):13224–13234

Liu FM, Yi SP, Ma HY, Huang JY, Tang YK, Qin JB, Zhou WH (2019) Risk assessment of groundwater environmental contamination: a case study of a karst site for the construction of a fossil power plant. Environ Sci Pollut R 26(30):30561–30574

Loke MH, Acworth I, Dahlin T (2003) A comparison of smooth and blocky inversion methods in 2D electrical imaging surveys. Explor Geophys 34(3):182–187

Loke MH, Barker RD (1996) Rapid least-squares inversion of apparent resistivity pseudosections by a quasi-Newton method. Geophys Prospect 44:131–152

Loke MH, Wilkinson PB, Chambers JE (2010) Fast computation of optimized electrode arrays for 2D resistivity surveys. Comput Geosci 36(11):1414–1426

Mao D, Lu L, Revil A, Zuo Y, Hinton J, Ren ZJ (2016) Geophysical monitoring of hydrocarbon-contaminated soils remediated with a bioelectrochemical system. Environ Sci Technol 50:8205–8213

Mao DQ, Wang XD, Meng J, Ma XM, Jiang XW, Wan L, Yan HB, Fan Y (2022) Infiltration assessments on top of yungang grottoes by time-lapse electrical resistivity tomography. Hydrology 9(5):77

Mary B, Sottani A, Boaga J, Camerin I, Deiana R, Cassiani G (2023) Non-invasive investigations of closed landfills: an example in a karstic area. Sci Total Environ 905:167083

Maurya PK, Ronde VK, Fiandaca G, Balbarini N, Auken E, Bjerg PL, Christiansen AV (2017) Detailed landfill leachate plume mapping using 2D and 3D electrical resistivity tomography - with correlation to ionic strength measured in screens. J Appl Geophys 138:1–8

McCall W, Christy TM (2020) The hydraulic profiling tool for hydrogeologic investigation of unconsolidated formations. Ground Water Monit R 40(3):89–103

McDnonald MG, Harbaugh AE (1988) A modeular three-dimensional finite- difference groundwater flow model. US Geological Survey Open File Report, 83–875 chap. A1 586 p.

Meng J, Dong YH, Xia T, Ma XM, Gao CL, Mao DQ (2022a) Detailed LNAPL plume mapping using electrical resistivity tomography inside an industrial building. Acta Geophys 70(4):1651–1663

Meng J, Zhang JM, Mao DQ, Han CM, Guo LL, Li SP, Chao C (2022b) Organic contamination distribution constrained with induced polarization at a waste disposal site. Water 14(22):3630

Naudet V, Revil A, Rizzo E, Bottero JY, Bégassat P (2004) Groundwater redox conditions and conductivity in a contaminant plume from geoelectrical investigations. Hydrol Earth Syst Sci 8(1):8–22

Orellana-Macías JM, Roselló MJP, Causapé J (2021) A methodology for assessing groundwater pollution hazard by nitrates from agricultural sources: application to the Gallocanta Groundwater Basin (Spain). Sustain 13(11):6321

Persaud E, Levison J (2021) Impacts of changing watershed conditions in the assessment of future groundwater contamination risk. J Hydrol 603(D):127142.

Revil A, Glover PWJ (1997) Theory of ionic-surface electrical conduction in porous media. Phys Rev B 55(3):1757–1773

Rogers KM, Van der Raaij R, Phillips A, Stewart M (2023) A national isotope survey to define the sources of nitrate contamination in New Zealand freshwaters. J Hydrol 617(C):129131

Sankoh AA, Laar C, Derkyi NSA, Frazer-Williams R (2023) Application of stable isotope of water and a Bayesian isotope mixing model (SIMMR) in groundwater studies: a case study of the Granvillebrook and Kingtom dumpsites. Environ Monit Assess 195(5):548

Sanuade OA, Arowoogun KI, Amosun JO (2022) A review on the use of geoelectrical methods for characterization and monitoring of contaminant plumes. Acta Geophys 70(5):2099–2117

Siddiqua A, Hahladakis JN, Al-Attiya WAKA (2022) An overview of the environmental pollution and health effects associated with waste landfilling and open dumping. Environ Sci Pollut R 29(39):58514–58536

Sims JL, Stroski KM, Kim S, Killeen G, Ehalt R, Simcik MF, Brooks BW (2022) Global occurrence and probabilistic environmental health hazard assessment of per- and polyfluoroalkyl substances (PFASs) in groundwater and surface waters. Sci Total Environ 816:151535

Torkashvand M, Neshat A, Javadi S, Pradhan B (2021) New hybrid evolutionary algorithm for optimizing index-based groundwater vulnerability assessment method. J Hydrol 598:126446

Wilkinson PB, Meldrum PI, Chambers JE, Kuras O, Ogilvy RD (2006) Improved strategies for the automatic selection of optimized sets of electrical resistivity tomography measurement configurations. Geophys J Int 167(3):1119–1126

Xia T, Dong Y, Mao D, Meng J (2021) Delineation of LNAPL contaminant plumes at a former perfumery plant using electrical resistivity tomography. Hydrogeol J 29(3):1189–1201

Xu BW, Noel M (1993) On the completeness of data sets with multi-electrode systems for electrical-resistivity survey. Geophys Prospect 41(6):791–801

Yin X, Jiang BL, Feng ZX, Yao BK, Shi XQ, Sun YY, Wu JC (2017) Comprehensive evaluation of shallow groundwater quality in Central and Southern Jiangsu Province China. Environ Earth Sci 76(11):400

Yu SY, Lee PK, Huang SI (2015) Groundwater contamination with volatile organic compounds in urban and industrial areas: analysis of co-occurrence and land use effects. Environ Earth Sci 74(4):3661–3677

Zhai Y, Zhao X, Teng Y, Li X, Zhang J, Wu J, Zuo R (2017) Groundwater nitrate pollution and human health risk assessment by using HHRA model in an agricultural area, NE China. Ecotoxicol Environ Saf 137:130–142

Zheng C, Wang PP (1999) MT3DMS: a modular three-dimensional multispecies transport model for simulation of advection, depersion and chemical reactions of contaminants in groundwater systems. Documentation and User's Guide, Contract Report SERDP-99–1, U.S. Army Engineer Research and Development Center